

Multi-Camera Collaborative Depth Prediction via Consistent Structure Estimation

Jialei Xu
Harbin Institute of Technology
Harbin, China
21b903029@stu.hit.edu.cn

Xianming Liu*
Harbin Institute of Technology &
Peng Cheng Laboratory
Harbin, China
csxm@hit.edu.cn

Yuanchao Bai
Harbin Institute of Technology
Harbin, China
yuanchao.bai@hit.edu.cn

Junjun Jiang
Harbin Institute of Technology &
Peng Cheng Laboratory
Harbin, China
jiangjunjun@hit.edu.cn

Kaixuan Wang
Shenzhen DJI Sciences and
Technologies Ltd.
Shenzhen, China
halfbullet.wang@dji.com

Xiaozhi Chen
Shenzhen DJI Sciences and
Technologies Ltd.
Shenzhen, China
xiaozhi.chen@dji.com

Xiangyang Ji
Tsinghua University
Beijing, China
xyji@tsinghua.edu.cn

ABSTRACT

Depth map estimation from images is an important task in robotic systems. Existing methods can be categorized into two groups including multi-view stereo and monocular depth estimation. The former requires cameras to have large overlapping areas and sufficient baseline between cameras, while the latter that processes each image independently can hardly guarantee the structure consistency between cameras. In this paper, we propose a novel multi-camera collaborative depth prediction method that does not require large overlapping areas while maintaining structure consistency between cameras. Specifically, we formulate the depth estimation as a weighted combination of depth basis, in which the weights are updated iteratively by a refinement network driven by the proposed consistency loss. During the iterative update, the results of depth estimation are compared across cameras and the information of overlapping areas is propagated to the whole depth maps with the help of basis formulation. Experimental results on DDAD and NuScenes datasets demonstrate the superior performance of our method.

CCS CONCEPTS

• **Computing methodologies** → **Scene understanding.**

*Corresponding author.

Permission to make digital or hard copies of all or part of this work for personal or classroom use is granted without fee provided that copies are not made or distributed for profit or commercial advantage and that copies bear this notice and the full citation on the first page. Copyrights for components of this work owned by others than ACM must be honored. Abstracting with credit is permitted. To copy otherwise, or republish, to post on servers or to redistribute to lists, requires prior specific permission and/or a fee. Request permissions from permissions@acm.org.

MM '22, October 10–14, 2022, Lisboa, Portugal.

© 2022 Association for Computing Machinery.

ACM ISBN 978-1-4503-9203-7/22/10...\$15.00

<https://doi.org/10.1145/3503161.3548394>

KEYWORDS

Depth estimation, multi-camera, 3D perception

ACM Reference Format:

Jialei Xu, Xianming Liu*, Yuanchao Bai, Junjun Jiang, Kaixuan Wang, Xiaozhi Chen, and Xiangyang Ji. 2022. Multi-Camera Collaborative Depth Prediction via Consistent Structure Estimation. In *Proceedings of the 30th ACM International Conference on Multimedia (MM '22)*, October 10–14, 2022, Lisboa, Portugal. ACM, New York, NY, USA, 9 pages. <https://doi.org/10.1145/3503161.3548394>

1 INTRODUCTION

Generating high-fidelity depth from color is attractive due to that it offers an inexpensive alternative to complement LIDAR sensors. Depth estimation enables agents to reconstruct the surrounding 3D environment, and thus holds great potential applications in self-driving cars, robotics, AR-compositing, etc.

Depth estimation without knowing a reference input image is an ill-posed problem. To produce dense depth, the current methods typically take as input synchronized stereo pairs or a monocular stream of images, which are referred to as multi-view stereo (MVS) [14, 33, 36] and monocular depth prediction [9, 13, 40], respectively. MVS based methods estimate the depth of every pixel using the constrains from multi-view geometry. One pixel has to be observed by multiple cameras distributed in space. The overlap of cameras and baseline between cameras are important for the estimation accuracy. For example, KITTI dataset [11] are collected by a multi-camera systems with a baseline of 0.54m, which limits the application of consuming products. Monocular depth prediction, on the other hand, uses deep learning methods to infer the depth map from only one image. The scale information is unobservable in images such that depth maps of different cameras can hardly be consistent to each other. Inconsistence between cameras will lead to poor reconstruction and downstream tasks.

The modern self-driving cars are usually equipped with multiple cameras to capture the full surround 360° field of view. This

inspires a new line of depth estimation, which works in a multi-camera setting by leveraging cross-camera overlapping contexts. Different from the stereo pair based methods, instead of requiring stereo-rectified or highly-overlapping images, it rather exploits small overlaps (as low as 10%) between cameras with arbitrary locations [16]. Surprisingly, there are very few works along this way. To the best of our knowledge, there are only two existing works in the literature so far [16, 34]. Guizilini *et al.* propose the first work along this line, referred to as full surround monodepth (FSM) [16], which leverages cross-camera temporal contexts via spatio-temporal photometric constraints to increase the amount of overlap between cameras. By exploiting known extrinsics between cameras, FSM enforces pose consistency constraints to ensure all cameras follow the same rigid body motion. However, the photometric loss [13] cross cameras used by FSM can be affected by brightness change or lens distortion. In addition, it can only utilize the information of the overlapping parts between multiple cameras in the training phase. In the inference stage, images are processed independently and the overlapping parts are ignored. In challenging scenes, the depth consistency will be violated, leading to poor depth estimation accuracy.

In this paper, we propose a novel multi-camera collaborative depth prediction (MCDP) method that can recover the absolute scale and maintain the structure consistency between multiple cameras, without the requirement of large camera overlapping. Specifically, we formulate the depth estimation as a weighted combination of depth basis, in which the weights are updated iteratively by a refinement network driven by the proposed structure consistency loss. During the iterative update, we align the results of depth estimation across cameras and extract the features of overlapping areas to guide the refinement of the weights, such that the information of small overlapping areas can be propagated to the whole depth maps with the help of basis formulation. We evaluate the effectiveness of our method on the widely used DDAD [13] and NuScenes [5] datasets. The contributions of this work can be summarized as follows:

- We introduce a novel multi-camera collaborative depth prediction method that can exploit small overlapping information between cameras to achieve scale and structure consistency of depth predictions.
- To improve the efficiency and reduce the network parameters, we solve the depth estimation problem through a basis combination scheme, which is referred to as depth basis for consistent structure estimation. The depth basis is estimated for each specific image and the weights are updated by multi-view information.
- We demonstrate the effectiveness of the proposed approach on two public multi-camera datasets: DDAD [13] and NuScenes [5]. The proposed approach achieves the state-of-the-art performance compared with other approaches.

2 RELATED WORK

2.1 Monocular Depth Estimation

Relying on the depth ground-truth, Eigen *et al.* [6] develop an architecture for coarse-to-fine depth estimation with a scale-invariant

loss function. This pioneering work inspires new CNN-based architectures to monodepth estimation [17, 23, 37, 39]. Supervised monocular depth prediction needs to use the ground-truth provided by the depth sensor as the supervision information. In the existing datasets such as NYU [29] and KITTI [10], depth sensors commonly use stereo cameras and LiDAR to get depth information. With the development of the depth prediction network, supervised depth estimation tries to use classification problem [3, 8] to predict depth, which has achieved very good results. With the great breakthrough of the transformer network structure in computer vision, [27, 35] adopts the model related to the transformer, and have made great progress in many datasets. As a perceptual algorithm, depth prediction need strong geometric constraints. [19, 38] use the coplanar constraint of normal vectors and points to strengthen the geometry.

The drawback of these supervised approaches is that the depth ground truth usually comes from the expensive LiDAR, which must be calibrated and synchronized with the cameras. Moreover, LiDAR depth is sparse compared to available image resolutions. In many outdoor scenes, the surface of objects such as glass and water will affect the range detection of LiDAR. Therefore, the self-supervised depth estimation model receives more and more attention.

[24] provides a pivotal principle of self-supervised, which has affected the design of many models so far. Their key idea is that obtaining a frame X_t from consecutive ones, and $\{X_{t-1}, X_{t+1}\}$ can be decomposed into jointly estimating the scene depth for X_t and the camera pose at time T relative to its pose at time $t \pm 1$. Zhou *et al.* [40] follow this idea. They train the depth network to estimate depth map from the X_t and the pose network to estimate the pose between the X_t and $X_{t \pm 1}$. The photometric loss between X_t and \hat{X}_t acts as training loss. Furthermore, Godard *et al.* [13] propose a model called Mono2, where the multi-scale approach and per-pixel minimum reprojection loss are adopted for the better handling of occlusions. Mono2 has achieved a huge breakthrough, providing a standard framework for subsequent monocular deep self-supervised tasks. A large number of subsequent tasks are launched with Mono2 as the benchmark. Based on Mono2, Watson *et al.* [33] combine the strengths of monocular and multi-view depth estimation at test time. They introduce efficient losses to improve the accuracy of the moving objects. Guizilini [15] propose a new convolutional network architecture called PackNet, which is available for high-resolution, and introduce a novel loss that can optionally leverage the camera's velocity.

2.2 Multi-Camera Depth Estimation

Multi-camera depth prediction includes stereo matching and multi view stereo. Stereo matching has been an active field of research for decades [28]. Traditional methods utilize handcrafted schemes to find local correspondences [18]. Recently, based on the deep learning, Goard *et al.* [12] take networks to estimate depth with left-right consistency. [30] propose a fast multi-resolution initialization step that computes high resolution matches using learned features. However stereo pairs need two cameras being coplanar after rectifying. Multi view stereo reconstruct 3D information of the scene from pictures of different angles. Gu *et al.* [14] apply the cascade cost volume to the MVS-Net, and achieves the best performance on the benchmark. Yang *et al.* [36] propose a cost-volume based, compact,



Figure 1: Examples and the overlapping areas of each camera on the DDAD dataset. First row: RGB images of cameras. Second Rows: Synthesized images warped from adjacent cameras.



Figure 2: Synthesized images across cameras.

and computational efficient depth inference network for MVS. Their framework can handle high resolution images with less memory requirement, and achieve a better accuracy. Khot *et al.* [20] propose a self-supervised multi-view stereo architecture using only images from novel views as supervisory signal. Although these approaches achieve very empirical results, these schemes require large areas of overlap between images. The reduction in the overlap range can have a very serious impact on these methods. Guizilini *et al.* [16] innovatively propose full surround monocular depth estimation from multiple cameras in autonomous driving scenarios. By studying spatial-temporal contexts, pose consistency constraints and the effects of overlapping, they open a new direction for multi-camera depth estimation.

3 METHODOLOGY

To motivate the design of multi-camera depth estimation approach under the circumstance of small camera overlapping, we first describe the strength and weakness of existing approaches in Sec. 3.1. We next explain our approach by extending the single-camera monocular self-supervised depth estimation to multi-camera setting in Sec. 3.2. Our approach can effectively estimate depth maps while maintain structure consistency between different cameras.

3.1 Motivation

It is challenging to perform multi-camera depth estimation where only small overlapping areas (as low as 10%) exist. Recent method FSM [16] proposes a feasible solution based on the standard self-supervised depth monocular estimation, and imposes the constraints on the loss of multi-camera spatio-temporal contexts and multi-camera pose consistency. As shown in Fig. 2, for two cameras C^i and C^j with overlapping areas, FSM computes the photometric loss between I^i and the synthesized image $I^{j \rightarrow i}$ from camera C^j at the same frame. However, such approach suffers from some limitations.

By comparing Fig. 2b and Fig. 2c, although the structures of the two images in the overlapping area is consistent with each other, there exists significant difference with respect to the brightness level. Besides, some objects existing in one camera are obscured in another camera, due to the large camera placement angle. Limited by these undesirable artifacts, the synthesized picture cannot be used as an effective supervision signal. In addition, FSM only conducts multi-camera collaboration in the training phase while degrades to a single-camera monocular depth estimation approach in the inference phase, which also leads to ineffective exploitation of the information across multiple cameras.

3.2 Our Approach

Motivated by the above analysis, we propose an effective scheme to fully employ the cross-camera correlation information in both the training and inference phases. The overall framework of the proposed approach is illustrated in Fig. 3.

3.2.1 Self-supervised Monocular Depth Estimation. We first adopt self-supervised monocular depth estimation to predict the depth map from a RGB image without ground-truth, inspired by [13]. Given a single input image I_t , we train a baseline network to predict its corresponding depth map D_t . The pose network takes temporally adjacent images as input and estimates relative pose $T_{t \rightarrow t+n}$ between the target image I_t and source images I_{t+n} , $n \in \{-1, +1\}$. Based on the estimated depth D_t , the relative camera pose $T_{t \rightarrow t+n}$ and camera intrinsics matrix K , we perform view synthesis as the supervisory signal,

$$I_{t+n \rightarrow t} = I_{t+n} \langle \text{proj}(D_t, T_{t \rightarrow t+n}, K) \rangle. \quad (1)$$

Here $\text{proj}(\cdot)$ are the resulting 2D coordinates of the projected depths D_t in I_{t+n} , and $\langle \cdot \rangle$ is the sampling operator. This view synthesis operation is fully differentiable, enabling gradient back-propagation for end-to-end training. We train the self-supervised monocular depth estimation network by minimizing the per-pixel minimum photometric re-projection error L_p [13] between the actual target image I_t and $I_{t \rightarrow t+n}$

$$L_p = \min_{t+n} pe(I_t, I_{t+n \rightarrow t}), \quad (2)$$

where $pe(\cdot)$ denotes the photometric error consisting of L_1 error and the Structural Similarity (SSIM) [32]

$$pe(I_a, I_b) = \frac{\alpha}{2} (1 - \text{SSIM}(I_a, I_b)) + (1 - \alpha) \|I_a - I_b\|_1, \quad (3)$$

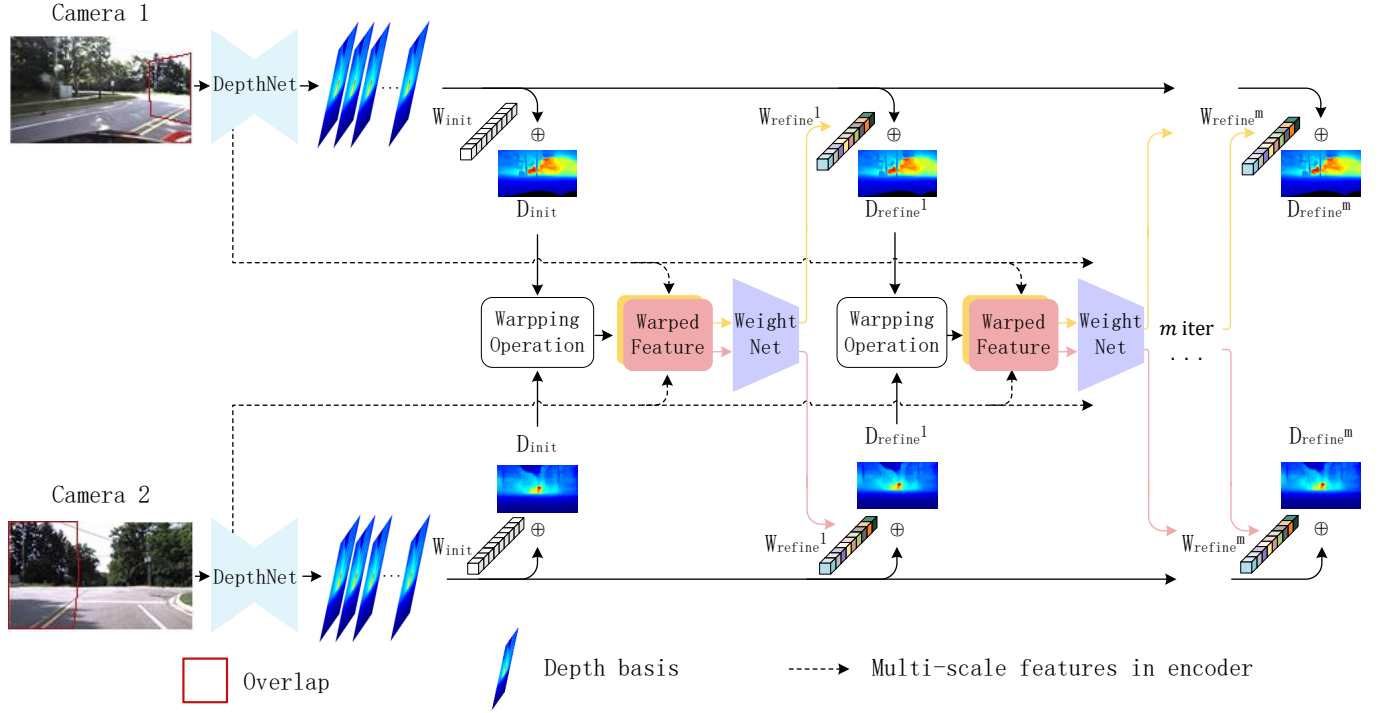


Figure 3: The architecture of the proposed multi-camera collaborative depth prediction via consistent structure estimation. Two adjacent cameras estimate the depth maps together. A warped feature contains all the features of one camera and the features of another camera in the overlapping part. The two warped features are respectively inputted into the weight network to calculate the weight of the corresponding camera. m is the refine times. After each refinement, an optimized depth map will be obtained, which is calculated by the linear combination \oplus of depth basis and weight. W_{init} and W_{refine^k} denote the initial weight and the weight of the k -th refinement.

where $\alpha = 0.85$. As in [12], we use edge-aware smoothness which calculates the mean-normalized inverse depth from [31] to discourage shrinking of the estimated depth.

3.2.2 Multi-Camera Collaborative Depth Prediction. Multi-camera approaches to self-supervised depth estimation are severely limited by camera placement setting. Stereo depth estimation methods [2, 22] need to rectify the images to predict the disparities with a known baseline. The approaches to multi-view stereo [14, 36] predict depth maps based on different camera positions to build the cost volume. Although these methods have been proposed to utilize the positional relationship and information between images, they all need a large overlapping areas in the images, such as KITTI [11], DTU [1] datasets.

Depth Basis for Consistent Structure Estimation. We propose the depth basis for consistent structure estimation to solve the problem of self-supervised depth estimation consistency with small overlapping areas in multi-camera systems. It can make more rational use of the overlapping images, and use the information of adjacent cameras to improve the accuracy of overall depth estimation in the inference stage.

Inspired by [4], the dense depth map can be adjusted by a small number of basic states, and we modify the architecture of monocular

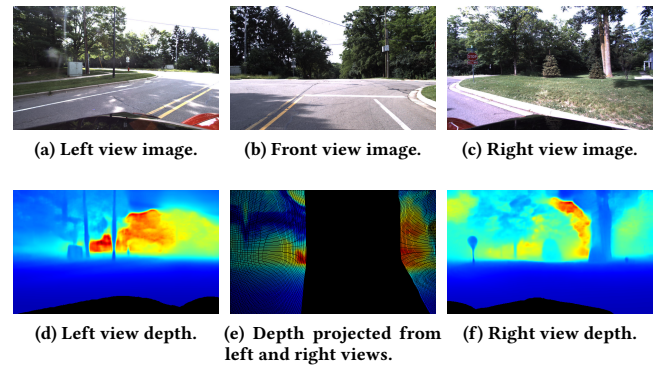


Figure 4: Depth projection from different views

depth estimation network. Specifically, the image I_t^i from camera C^i is fed to the modified depth estimation network to generate n depth bases $B^i \in \mathbb{R}^{n \times H \times W}$ instead of the depth, where H and W are the height and width of the input images. Each basis represents a state of possible distribution of the depth. The estimated depth map is the combination of the bases. We set n initial weights W_{init}^i

and calculate the initial depth D_{init}^i with B^i

$$D_{init}^i = B^i \oplus W_{init}^i = \sum_{j=1}^n w_{init}^{i,j} \cdot B^{i,j}, \quad (4)$$

where $w_{init}^{i,j}$ is the j -th element of W_{init}^i and $B^{i,j}$ is the j -th depth basis of B^i . For each camera, the initial weight $w_{init}^{i,j}$ is set to $\frac{1}{n}$. The size of D_{init}^i is $1 \times H \times W$, which is the same as each basis. The n depth bases enjoy more flexibility to express the depth, which provides a place to optimise. If we fix the initial weights W_{init}^i , there is no difference between generating depth directly and using bases to linearly compute depth as an optimization problem. Another advantage is that we only need to adjust the weights of bases to refine the combination instead of recalculating the depth map pixel by pixel. This greatly reduces the number of parameters and computational complexity. When more than one camera are available, the weight can be further optimized by exploiting the overlapping views between the target camera and the adjacent cameras.

Weight Network. We assume that the cameras are rigidly connected in the multi-camera setting, and obtain the extrinsics matrix $E^{i \rightarrow j}$ including $R^{i \rightarrow j}$ and $t^{i \rightarrow j}$ between each two cameras from the datasets. Combining intrinsics K of the standard pinhole model [25] and the estimated depth D , we obtain the pixel-warping operation between the camera C^i and C^j :

$$\hat{\mathbf{p}}^i = \pi_j(R^{i \rightarrow j} \phi_i(\mathbf{p}^i, D^i, K^i) + t^{i \rightarrow j}, K^j), \quad (5)$$

where $\phi(\mathbf{p}, D, K) = \mathbf{P}$ is the unprojection of a pixel in homogeneous coordinates \mathbf{p} to a 3D point \mathbf{P} for a given estimated depth D . $\pi(\mathbf{P}, K) = \mathbf{p}$ denotes the projection of a 3D point back onto the image plane.

To exploit the useful information of the overlapping parts, we warp feature maps of another view obtained by the encoder in the depth network. We first obtain features at three scales in the encoder, $H/2^i \times W/2^i$, ($i = 1, 2, 3$, $H \times W$ is the size of the input image). We use bilinear interpolation to align the multi-scale features to the same size $H/2 \times W/2$ and concatenate them along channels. Based on the pixel-warping operation between cameras (5), we warp the multi-scale features F^j from C^j to C^i . The non-overlapping area of the image is filled with 0. We concatenate the warped F^j with F^i , leading to the feature \hat{F}^i . In the view of C^i , \hat{F}^i has not only all the features of I^i , but also the multi-scale features of the overlapping part from I^j .

With the more informative feature \hat{F}^i , we propose to refine the combination of the depth basis in order to generate a higher quality depth map. We design a *weight network* in order to refine the weights for the combination of depth bases B^i . The input of the network is \hat{F}^i and the output is the refined weight W_{refine}^i . Thanks to the new features provided by adjacent cameras, the weight network can achieve a more accurate solution to the depth map estimation of the target view. We show the specific structure of the weight network in Fig. 5. With W_{refine}^i and B^i , we can generate the refined depth map D_{refine}^i with (4).

Iterative Refinement Strategy. After one refinement, we can get a more accurate depth map D_{refine}^i . According to (5), the quality of depth map impacts the pixel-warping operation, and the refined

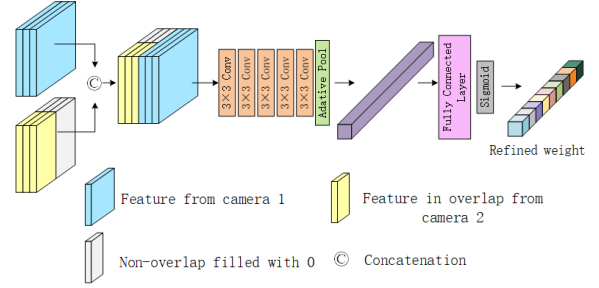


Figure 5: The architectures of the weight network

depth map can reduce the projection errors. We thus propose an iterative refinement strategy to use the refined depth map in the current step as the input of the next step, and repeat this process for m times. The images from different cameras share the same weight network in each step, but the networks of different steps are independent from each other. We analyze the effect of the number m of iterations in the experiments.

3.2.3 Loss Function. The overlap taken by the multi-camera predicts the depth map of each image. The consistency between multiple depth maps has a great impact on downstream tasks, such as autonomous driving. Low depth consistency can lead to semantic error, path planning deviation and so on. To achieve more consistent depth estimation for overlapping areas under different cameras, Fan *et al.* come up with *Chamfer Loss* [7], which can backproject the depth map to the world coordinate system. It improves consistency by minimizing the distance between two point clouds in overlapping areas. But the point cloud generated by the depth map backprojection is very dense. The resolution of the image is 1936×1216 in DDAD dataset [15], and there are more than 2 million points in one point cloud generated by an image. Although *chamfer distance* can be optimized by *KD Tree*, computation between point clouds consumes a lot of computing power. In our experiment, a standard depth network iteration spends 0.5 about seconds, but it spends over 10 seconds with *chamfer loss*.

Depth Consistency Loss. We design a depth consistency loss L_{con} to reduce the error between the estimated depth maps from different cameras in the overlap. Since the camera planes of different cameras are not coplanar, the depth maps estimated from different cameras cannot be directly compared. We project the depth values onto the same camera plane by (5). Instead of grid sampling and interpolation operation, we use the simple coordinate transformation. We can project D^j from C^j to C^i and generate a depth map \hat{D}^i with only overlapping areas predicted by the C^j . As shown in Fig. 4, the depth maps in Fig. 4d and 4f are estimated by the left view in Fig. 4a and right view in Fig. 4c respectively, and project them to front view in Fig. 4e. In the process of projecting the point cloud to the image plane, multiple points may be projected to the same pixel. Based on pixel order, the points projected later overwrite the points projected earlier, and pixels that are not projected to are filled with 0.

Under the same coordinate system, we can directly calculate the difference in depth for the overlapping areas. We L_1 loss to

constraint between D^i and \hat{D}^i . We denote depth consistency loss:

$$L_{con} = L_1(D^i, \hat{D}^i). \quad (6)$$

Full Loss. Just like the basic self-supervised monocular depth estimation method [13], we need to predict ego-motion in the image sequence to construct supervision according to (2). The pose network takes each temporally images $\{I_t^i, I_{t-1}^i, I_{t+1}^i\}$ from the camera C^i to estimate the pose $T_{t \rightarrow t+n}^i$. The depth estimation network is shared between cameras. During multi-camera self-supervised training, the full loss is comprised of the photometric loss L_p and depth consistency loss L_{con} . Because the depth maps resulting from the MCDP include initial depth map and multiple refined depth maps, the full loss takes the form:

$$L = L_p^{init} + \lambda L_{con}^{init} + \sum_{k=1}^m (L_p^k + \lambda L_{con}^k), \quad (7)$$

where λ is a hyper-parameter to balance the L_p and L_{con} , and m is the number of refinement steps. We assume that each refinement step contributes equally in (7).

4 EXPERIMENTS

4.1 Datasets

Traditionally, the methods of monocular self-supervised depth estimation are often verified on the KITTI dataset [11]. There are only rectified stereo pairs from forward-facing cameras in the KITTI. In recent years, some multi-camera omnidirectional autonomous driving datasets have been open sourced. For the setting of multiple cameras and a small amount of overlapping area, we choose the two datasets to validate our scheme.

DDAD [15]. The Dense Depth for Automated Driving (DDAD) is an urban driving dataset captured with six synchronized cameras with relatively small overlap. It contains highly accurate dense ground-truth depth maps for evaluation and max depth range is up to 250 meters. It has a total of 12650 training samples (63250 images) and 3950 validation samples (15800 images). In the training set, we do not use ground-truth depth maps. The resolution of the images is 1936×1216 . Following the procedure outlined in [16], input images are downsampled to the 640×384 resolution. For evaluation, we use bilinear interpolation to upsample the image resolution to the original size.

NuScenes [5]. The NuScenes dataset is an urban driving dataset that contains images from a synchronized six-camera array. It comprises of 1000 scenes with a total of 1.4 million images. It is a popular benchmark for 2D and 3D object detection, as well as semantic and instance segmentation. This dataset is challenging for self-supervised depth estimation task because of the relatively low resolution of the images, very small overlap between the cameras, high diversity of weather conditions and time of day, and unstructured environments. The size of raw images is 1600×900 , which are downsampled to 768×448 . The images are captured at 30Hz, and the samples of the dataset are annotated at 2Hz as key frames. Due to the large time interval of key frames, deep networks cannot be trained in a self-supervised manner. We use the sequences from the raw dataset as the supervisory signal, which are not annotated.

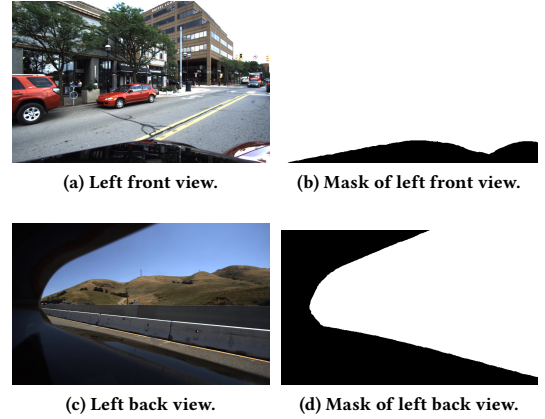


Figure 6: Self-Occlusions Mask.

4.2 Multi-Camera Depth Evaluation Metrics

We take the *median-scaling* [40] approach to evaluate the results, which is commonly used in self-supervised monodepth estimation at test time. Based on the proposed depth consistency loss, we design a new depth consistency metric *Dep Con* to evaluate depth consistency in the image plane:

$$Dep\ Con = \frac{|D^i - \hat{D}^i|}{D_{gt}}, \quad (8)$$

where D_{gt} is the ground-truth depth map. We project the depth maps of overlaps to the same camera plane by (5), and calculate the ratio of the absolute errors of D^i and \hat{D}^i to the ground-truth. The role of the ratio is to balance the effect of the prediction distance on the error. Instead of calculating distances between point clouds, we calculate the distance between two depth maps, which can significantly reduce computational complexity.

In addition to the proposed *Dep Con* metric, we use the standard four metrics used in the prior work [13]: average relative error (Abs Rel), squared relative difference (Sq Rel), root mean squared error (RMS), threshold accuracy ($\delta_{1.25}$).

4.3 Implementation details

We implement the proposed scheme in PyTorch [26], training networks for 20 epochs on two Nvidia RTX 3090 GPU. The batch size is set to 12 in DDAD dataset and 8 in NuScenes dataset. We jointly train the depth network, pose network and weight network with Adam Optimizer [21] with $\beta_1 = 0.9$, $\beta_2 = 0.999$. The initial learning rate is set to $1e^{-4}$ and decay for the first 15 epochs which is then dropped to $1e^{-5}$ for the remainder. We set the SSIM weight to $\alpha = 0.85$, the weight of smoothness term to 0.001, the weight of depth consistency loss to $\lambda = 0.001$ and the number of depth basis $n = 32$. Training takes 40 hours for DDAD dataset and 140 hours for NuScenes dataset. In the testing phase, we do not flip the image left and right and take the average, although this is used in many works [3, 35] to improve the accuracy.

Depth Estimation Network. Following the Mono2 [13], we use the ResNet18-based depth and pose networks for depth estimation. As

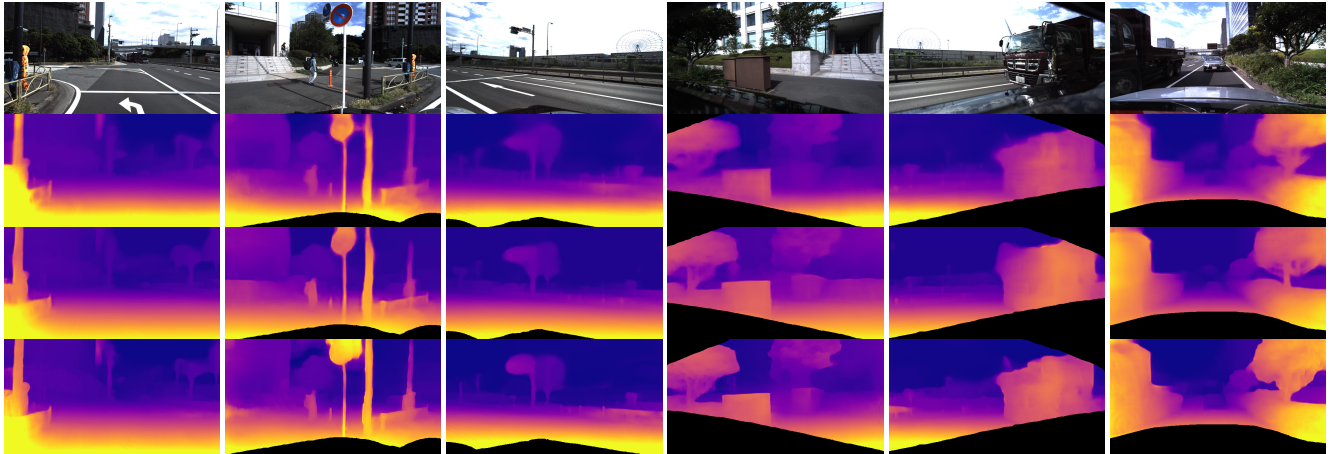


Figure 7: Qualitative results on the DDAD dataset. The first row: RGB pictures of six cameras. The second row: Mono2 [13]. The third row: FSM [16]. The fourth row: MCDP.

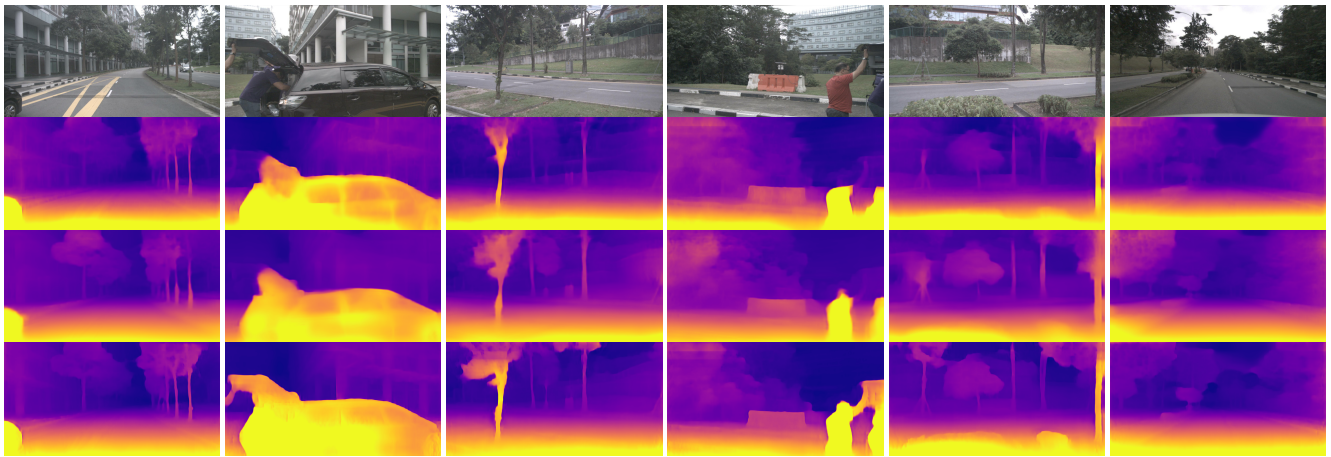


Figure 8: Qualitative results on the NuScenes dataset. The first row: RGB pictures of six cameras. The second row: Mono2 [13]. The third row: FSM [16]. The fourth row: MCDP.

the underlying network for monocular self-supervised estimation, the details are consistent with Mono2 and remain unchanged in all our experiments.

Self-Occlusions. As shown in Fig. 6, part of the images is obscured by the car itself, and the occluded area in multiple positions is very large. This occlusion has a serious impact on the calculation of the photometric loss. In addition, there are also self-occlusion in the overlap of multi-camera, which will also bring wrong guidance to the refinement work. Referring to [16] for dealing with occlusion, we manually draw the mask for each camera, which only needs to be drawn once for the entire dataset. In the calculation of L_p , L_{con} and \hat{F} , masks are used to remove the occluded parts, which can remove erroneous information for the network in advance.

4.4 Depth Estimation Performance

Refinement by Depth Basis. In the two datasets, we mix the pictures of all cameras together and train them by the same model. We

first evaluate the overall impact of different methods on six cameras. As shown in Tab. 1, we take Mono2 [13] as the benchmark, and the effect of mask is obvious. As described in 3.2.2, MCDP can greatly improve the performance of all metrics. With only one refine adjustment, the *Abs Rel* reduces from 0.217 to 0.197 (10.1%) on DDAD and 0.296 to 0.240 (23.3%) on NuScenes, and $\delta_{1.25}$ can improve from 0.808 to 0.767 (5.0%) on DDAD and from 0.672 to 0.716 (6.1%) on NuScenes. This proves that the MCDP can use the overlapping part to improve the overall prediction performance of the cameras.

Furthermore, the characteristic of multi-camera framework is that it can be optimized many times. We refine it twice, and the performance of the model has been further improved. The *abs rel* reduces from 0.197 to 0.193 on DDAD and from 0.237 to 0.240 on NuScenes. Another metric $\delta_{1.25}$ improves from 0.808 to 0.811 on DDAD and from 0.716 to 0.719 on NuScenes. This proves that multiple refinement iterations can further improve the model performance. In Fig. 7 and Fig. 8, we show the quantitative results

Table 1: Quantitative depth results on multi-camera datasets. All values are the average of six cameras. The distances are up to 200m in DDAD and 60m in Nuscenes. The symbol * denotes sharing median-scaling at the test time. m denotes the refine times. M denotes the removal of masking.

(a) DDAD					
Method	Abs Rel↓	Sq Rel↓	RMSE↓	$\delta_{1.25}$ ↑	
Mono2 - M [13]	0.358	4.549	14.774	0.600	
Mono2 [13]	0.220	4.235	14.125	0.751	
PackNet [15]	0.215	4.012	13.649	0.696	
FSM* [16]	0.208	4.276	13.561	0.809	
FSM [16]	0.202	3.267	13.530	0.803	
SurroundDepth [34]	0.200	3.392	12.270	0.740	
MCDP ($m = 0$)	0.217	3.832	13.451	0.767	
MCDP (w/o L_{con}, $m = 1$)	0.205	3.165	12.306	0.798	
MCDP ($m = 1$)	0.197	3.150	12.265	0.808	
MCDP ($m = 2$)	0.193	3.111	12.264	0.811	

(b) NuScenes					
Method	Abs Rel↓	Sq Rel↓	RMSE↓	$\delta_{1.25}$ ↑	
Mono2	0.309	3.453	8.012	0.663	
PackNet [15]	0.303	3.154	7.014	0.655	
FSM* [16]	0.275	3.182	6.908	0.682	
FSM [16]	0.270	3.185	6.832	6.689	
SurroundDepth [34]	0.245	3.067	6.835	0.719	
MCDP ($m = 0$)	0.296	3.076	7.578	0.672	
MCDP (w/o L_{con}, $m = 1$)	0.257	3.052	6.849	0.702	
MCDP ($m = 1$)	0.240	3.031	6.825	0.716	
MCDP ($m = 2$)	0.237	3.030	6.822	0.719	

Table 2: Depth consistency results of each camera on two datasets.

Dataset	Method	Dep Con↓					
		Front	F.Left	F.Right	B.Left	B.Right	Back
DDAD	Mono2	0.637	0.279	0.330	0.317	0.336	0.391
	MCDP	0.621	0.268	0.205	0.228	0.292	0.330
NuScenes	Mono2	0.279	0.337	0.316	0.354	0.277	0.351
	MCDP	0.255	0.318	0.244	0.301	0.240	0.337

Table 3: Quantitative depth results on KITTI dataset. m denotes the refine times.

Method	m	Abs Rel↓	Sq Rel↓	RMSE↓	$\delta_{1.25}$ ↑
Mono2 [13]	-	0.106	0.806	4.630	0.876
MCDP (w/o L_{con})	1	0.105	0.805	4.622	0.878
MCDP	2	0.102	0.798	4.619	0.880

separately in DDAD and NuScenes. Compared with Mono2 and FSM, our method can significantly improve the accuracy of object edge and overlapping area.

Assessment for Depth Consistency Loss. In the Tab. 1, we compare the effects before and after using L_{con} in two datasets. Compared with the benchmark, $Abs Rel$ can reduce from 0.220 to 0.217 (1.3%) in DDAD and from 0.303 to 0.296 (2.6%) with L_{con} . More importantly, L_{con} can be used in refinement to improve the performance of the model. In the MCDP scheme, we show the results before and after using L_{con} based on refining once, and $Abs Rel$ reduces from 0.205 to 0.197 (4.0%) in DDAD and 0.257 to 0.240 (7.0%) in NuScenes. This proves that the L_{con} can improve the performance of the model by constraining the depth of the overlap between cameras. Combined with our results, the MCDP can iteratively refine the estimated depth for many times, and generates the state-of-the-art models.

4.5 Depth Consistency Metric

The depth consistency in overlapping parts is our focus. We use Equation 8 to evaluate the depth consistency error of overlapping parts. As shown in Tab. 2, due to the different depth distribution caused by the camera position, the depth consistency between cameras varies greatly. Left and right view cameras have better consistency than front and back cameras. Compared with the benchmark, MCDP can effectively improve the depth consistency between cameras. This is verified on six cameras in the both datasets.

4.6 Assessment for Robustness

In order to verify the robustness of our method, we select more diverse data for testing. KITTI [11] is a stereo camera dataset, and it is not suitable for the setting of small overlapping areas between cameras that we are concerned about. As shown in Tab. 3, our method is also effective on KITTI. It should be noted that, compared to the other multi-camera datasets like DDAD and NuScenes, the biggest advantage of KITTI is its rectified stereo cameras, which can calculate the disparity between images. However, it is impossible with two cameras placed arbitrarily to compute disparity, and our universal approach cannot take advantage of this particular advantage. Our approach also shows good robustness with large overlap on KITTI.

5 CONCLUSION

In this paper, we extend monocular depth prediction to multi-camera depth prediction at any position. In extreme scenes where the overlapping area between cameras is very small, we propose a multi-camera joint depth estimation scheme. We introduce a series of key technologies to improve the effect of depth prediction: depth basis for consistent structure estimation allows the model to use overlapping area information in inference, and the depth consistency loss restricts the depth consistency among multi-camera. We demonstrate the capabilities of my approach and their parametric performance in two standard autonomous driving datasets.

6 ACKNOWLEDGMENTS

This work was supported by National Natural Science Foundation of China under Grants 61922027, 6207115 and 61932022, and in part by National Key Research and Development Project under Grant 2019YFE0109600.

REFERENCES

- [1] Henrik Aanæs, Rasmus Ramsbøl Jensen, George Vogiatzis, Engin Tola, and Anders Bjarholm Dahl. 2016. Large-scale data for multiple-view stereopsis. *International Journal of Computer Vision* 120, 2 (2016), 153–168.
- [2] Abhishek Badki, Alejandro Troccoli, Kihwan Kim, Jan Kautz, Pradeep Sen, and Orazio Gallo. 2020. Bi3d: Stereo depth estimation via binary classifications. In *Proceedings of the IEEE/CVF Conference on Computer Vision and Pattern Recognition*. 1600–1608.
- [3] Shariq Farooq Bhat, Ibraheem Alhashim, and Peter Wonka. 2021. Adabins: Depth estimation using adaptive bins. In *Proceedings of the IEEE/CVF Conference on Computer Vision and Pattern Recognition*. 4009–4018.
- [4] Michael Bloesch, Jan Czarnowski, Ronald Clark, Stefan Leutenegger, and Andrew J Davison. 2018. CodeSLAM—learning a compact, optimisable representation for dense visual SLAM. In *Proceedings of the IEEE conference on computer vision and pattern recognition*. 2560–2568.
- [5] Holger Caesar, Varun Bankiti, Alex H Lang, Sourabh Vora, Venice Erin Liong, Qiang Xu, Anush Krishnan, Yu Pan, Giancarlo Baldan, and Oscar Beijbom. 2020. nuscenes: A multimodal dataset for autonomous driving. In *Proceedings of the IEEE/CVF conference on computer vision and pattern recognition*. 11621–11631.
- [6] David Eigen, Christian Puhrsch, and Rob Fergus. 2014. Depth map prediction from a single image using a multi-scale deep network. *Advances in neural information processing systems* 27 (2014).
- [7] Haoqiang Fan, Hao Su, and Leonidas J Guibas. 2017. A point set generation network for 3d object reconstruction from a single image. In *Proceedings of the IEEE conference on computer vision and pattern recognition*. 605–613.
- [8] Huan Fu, Mingming Gong, Chaohui Wang, Kayhan Batmanghelich, and Dacheng Tao. 2018. Deep ordinal regression network for monocular depth estimation. In *Proceedings of the IEEE conference on computer vision and pattern recognition*. 2002–2011.
- [9] Ravi Garg, Vijay Kumar Bg, Gustavo Carneiro, and Ian Reid. 2016. Unsupervised cnn for single view depth estimation: Geometry to the rescue. In *European conference on computer vision*. Springer, 740–756.
- [10] Andreas Geiger, Philip Lenz, Christoph Stiller, and Raquel Urtasun. 2013. Vision meets robotics: The kitti dataset. *The International Journal of Robotics Research* 32, 11 (2013), 1231–1237.
- [11] Andreas Geiger, Philip Lenz, and Raquel Urtasun. 2012. Are we ready for autonomous driving? the kitti vision benchmark suite. In *2012 IEEE conference on computer vision and pattern recognition*. IEEE, 3354–3361.
- [12] Clément Godard, Oisín Mac Aodha, and Gabriel J Brostow. 2017. Unsupervised monocular depth estimation with left-right consistency. In *Proceedings of the IEEE conference on computer vision and pattern recognition*. 270–279.
- [13] Clément Godard, Oisín Mac Aodha, Michael Firman, and Gabriel J Brostow. 2019. Digging into self-supervised monocular depth estimation. In *Proceedings of the IEEE/CVF International Conference on Computer Vision*. 3828–3838.
- [14] Xiaodong Gu, Zhiwen Fan, Siyu Zhu, Zuoqun Dai, Feitong Tan, and Ping Tan. 2020. Cascade cost volume for high-resolution multi-view stereo and stereo matching. In *Proceedings of the IEEE/CVF Conference on Computer Vision and Pattern Recognition*. 2495–2504.
- [15] Vitor Guizilini, Rares Ambrus, Sudeep Pillai, Allan Raventos, and Adrien Gaidon. 2020. 3d packing for self-supervised monocular depth estimation. In *Proceedings of the IEEE/CVF Conference on Computer Vision and Pattern Recognition*. 2485–2494.
- [16] Vitor Guizilini, Igor Vasiljevic, Rares Ambrus, Greg Shakhnarovich, and Adrien Gaidon. 2022. Full Surround Monodepth From Multiple Cameras. *IEEE Robotics and Automation Letters* 7, 2 (2022), 5397–5404. <https://doi.org/10.1109/LRA.2022.3150884>
- [17] Lei He, Guanghui Wang, and Zhanyi Hu. 2018. Learning depth from single images with deep neural network embedding focal length. *IEEE Transactions on Image Processing* 27, 9 (2018), 4676–4689.
- [18] Asmaa Hosni, Christoph Rhemann, Michael Bleyer, Carsten Rother, and Margrit Gelautz. 2012. Fast cost-volume filtering for visual correspondence and beyond. *IEEE Transactions on Pattern Analysis and Machine Intelligence* 35, 2 (2012), 504–511.
- [19] Benjamin Keltjens, Tom van Dijk, and Guido de Croon. 2021. Self-Supervised Monocular Depth Estimation of Untextured Indoor Rotated Scenes. *arXiv preprint arXiv:2106.12958* (2021).
- [20] Tejas Khot, Shubham Agrawal, Shubham Tulsiani, Christoph Mertz, Simon Lucey, and Martial Hebert. 2019. Learning unsupervised multi-view stereopsis via robust photometric consistency. *arXiv preprint arXiv:1905.02706* (2019).
- [21] Diederik P Kingma and Jimmy Ba. 2014. Adam: A method for stochastic optimization. *arXiv preprint arXiv:1412.6980* (2014).
- [22] Uday Kusupati, Shuo Cheng, Rui Chen, and Hao Su. 2020. Normal assisted stereo depth estimation. In *Proceedings of the IEEE/CVF Conference on Computer Vision and Pattern Recognition*. 2189–2199.
- [23] Fayao Liu, Chunhua Shen, Guosheng Lin, and Ian Reid. 2015. Learning depth from single monocular images using deep convolutional neural fields. *IEEE transactions on pattern analysis and machine intelligence* 38, 10 (2015), 2024–2039.
- [24] Onur Özyeşil, Vladislav Voroninski, Ronen Basri, and Amit Singer. 2017. A survey of structure from motion*. *Acta Numerica* 26 (2017), 305–364.
- [25] GF Page. 2005. MULTIPLE VIEW GEOMETRY IN COMPUTER VISION, by Richard Hartley and Andrew Zisserman, CUP, Cambridge, UK, 2003, vi+ 560 pp., ISBN 0-521-54051-8.(Paperback£ 44.95). *Robotica* 23, 2 (2005), 271–271.
- [26] Adam Paszke, Sam Gross, Francisco Massa, Adam Lerer, James Bradbury, Gregory Chanan, Trevor Killeen, Zeming Lin, Natalia Gimelshein, Luca Antiga, et al. 2019. Pytorch: An imperative style, high-performance deep learning library. *Advances in neural information processing systems* 32 (2019).
- [27] René Ranftl, Alexey Bochkovskiy, and Vladlen Koltun. 2021. Vision transformers for dense prediction. In *Proceedings of the IEEE/CVF International Conference on Computer Vision*. 12179–12188.
- [28] Daniel Scharstein and Richard Szeliski. 2002. A taxonomy and evaluation of dense two-frame stereo correspondence algorithms. *International journal of computer vision* 47, 1 (2002), 7–42.
- [29] Nathan Silberman, Derek Hoiem, Pushmeet Kohli, and Rob Fergus. 2012. Indoor segmentation and support inference from rgbd images. In *European conference on computer vision*. Springer, 746–760.
- [30] Vladimir Tankovich, Christian Hane, Yinda Zhang, Adarsh Kowdle, Sean Fanello, and Sofien Bouaziz. 2021. Hitnet: Hierarchical iterative tile refinement network for real-time stereo matching. In *Proceedings of the IEEE/CVF Conference on Computer Vision and Pattern Recognition*. 14362–14372.
- [31] Chaoyang Wang, José Miguel Buenaposada, Rui Zhu, and Simon Lucey. 2018. Learning depth from monocular videos using direct methods. In *Proceedings of the IEEE conference on computer vision and pattern recognition*. 2022–2030.
- [32] Zhou Wang, Alan C Bovik, Hamid R Sheikh, and Eero P Simoncelli. 2004. Image quality assessment: from error visibility to structural similarity. *IEEE transactions on image processing* 13, 4 (2004), 600–612.
- [33] Jamie Watson, Oisín Mac Aodha, Victor Prisacariu, Gabriel Brostow, and Michael Firman. 2021. The temporal opportunist: Self-supervised multi-frame monocular depth. In *Proceedings of the IEEE/CVF Conference on Computer Vision and Pattern Recognition*. 1164–1174.
- [34] Yi Wei, Lingqing Zhao, Wenzhao Zheng, Zheng Zhu, Yongming Rao, Guan Huang, Jiwen Lu, and Jie Zhou. 2022. SurroundDepth: Entangling Surrounding Views for Self-Supervised Multi-Camera Depth Estimation. *arXiv preprint arXiv:2204.03636* (2022).
- [35] Jialei Xu, Yuanhao Bai, Xianming Liu, Junjun Jiang, and Xiangyang Ji. 2021. Weakly-Supervised Monocular Depth Estimation with Resolution-Mismatched Data. *arXiv preprint arXiv:2109.11573* (2021).
- [36] Jiayu Yang, Wei Mao, Jose M Alvarez, and Miaomiao Liu. 2020. Cost volume pyramid based depth inference for multi-view stereo. In *Proceedings of the IEEE/CVF Conference on Computer Vision and Pattern Recognition*. 4877–4886.
- [37] Wei Yin, Yifan Liu, and Chunhua Shen. 2021. Virtual Normal: Enforcing Geometric Constraints for Accurate and Robust Depth Prediction. *IEEE Transactions on Pattern Analysis and Machine Intelligence (TPAMI)* (2021).
- [38] Wei Yin, Yifan Liu, Chunhua Shen, and Youliang Yan. 2019. Enforcing geometric constraints of virtual normal for depth prediction. In *Proceedings of the IEEE/CVF International Conference on Computer Vision*. 5684–5693.
- [39] Wei Yin, Jianming Zhang, Oliver Wang, Simon Niklaus, Long Mai, Simon Chen, and Chunhua Shen. 2021. Learning to Recover 3D Scene Shape from a Single Image.
- [40] Tinghui Zhou, Matthew Brown, Noah Snavely, and David G Lowe. 2017. Unsupervised learning of depth and ego-motion from video. In *Proceedings of the IEEE conference on computer vision and pattern recognition*. 1851–1858.